SPECIAL TOPIC: Graphene Oxides towards Practical Applications

Capillary shrinkage of graphene oxide hydrogels

Changsheng Qi[1,4†], Chong Luo[2†], Ying Tao[1,4†], Wei Lv[2], Chen Zhang[3], Yaqian Deng[2], Huan Li[1,4], Junwei Han[1,4], Guowei Ling[3] and Quan-Hong Yang[1,4*]

ABSTRACT   Conventional carbon materials cannot combine high density and high porosity, which are required in many applications, typically for energy storage under a limited space. A novel highly dense yet porous carbon has previously been produced from a three-dimensional (3D) reduced graphene oxide (r-GO) hydrogel by evaporation-induced drying. Here the mechanism of such a network shrinkage in r-GO hydrogel is specifically illustrated by the use of water and 1,4-dioxane, which have a sole difference in surface tension. As a result, the surface tension of the evaporating solvent determines the capillary forces in the nanochannels, which causes shrinkage of the r-GO network. More promisingly, the selection of a solvent with a known surface tension can precisely tune the microstructure associated with the density and porosity of the resulting porous carbon, rendering the porous carbon materials great potential in practical devices with high volumetric performance.

Keywords: graphene oxides, porous carbons, hydrogels, capillary force, network shrinkage

INTRODUCTION

Graphene, a single layer of carbon atoms arranged in a honeycomb network, has unique and versatile properties and can be considered as the building block of carbon materials [1]. For example, zero-dimensional (0D) fullerene can be regarded as a sphere of monolayer graphene and a one-dimensional (1D) carbon nanotube can be considered as a rolled graphene sheet [2]. As for conventional three-dimensional (3D) carbon materials, there are two factors involved in their structures, the stacking and packing of the sheets. As illustrated in Fig. 1, face-to-face parallel stacking produces a high density but non-porous carbon, like graphite, while edge-to-edge random packing results in porous carbon structures with high porosity but low density [3]. Graphite materials with stacked graphene sheets have a high density but show an electrochemical activity only for lithium and potassium ions [4,5]. Although carbon materials with random packing have an interconnected pore network and sufficient channels for ion transport, their low packing density and poor volumetric performance restrict their practical use in energy storage devices [6]. It is therefore hard for conventional carbon materials to achieve both high density and high porosity through the traditional assembly of carbon layers.

With the rapid development of portable electronics and electric vehicles, exploring materials with high volumetric performance is essential for energy storage [7,8]. Highly porous yet dense materials would deliver a high volumetric performance which is important for energy storage. However, using conventional strategies [9–11], it is hard to obtain materials with both high density and large surface area. Our previous study has demonstrated that graphene oxide (GO) can be used to produce highly porous but dense carbon monoliths, which are promising materials for compact energy storage highlighting volumetric performance [7,12–18]. GO as the oxidative exfoliation product of graphite is an amphiphile, due to its hydrophobic benzene-ring basal plane and the hydro-

[1] Nanoyang Group, State Key Laboratory of Chemical Engineering, School of Chemical Engineering and Technology, Collaborative Innovation Center of Chemical Science and Engineering (Tianjin), Tianjin University, Tianjin 300350, China
[2] Shenzhen Geim Graphene Center and Engineering Laboratory for Functionalized Carbon Materials, Graduate School at Shenzhen, Tsinghua University, Shenzhen 518055, China
[3] School of Marine Science and Technology, Tianjin University, Tianjin 300350, China
[4] Joint School of National University of Singapore and Tianjin University, International Campus of Tianjin University, Binhai New City, Fuzhou 350207, China
[†] These authors are equal major contributors to this work.
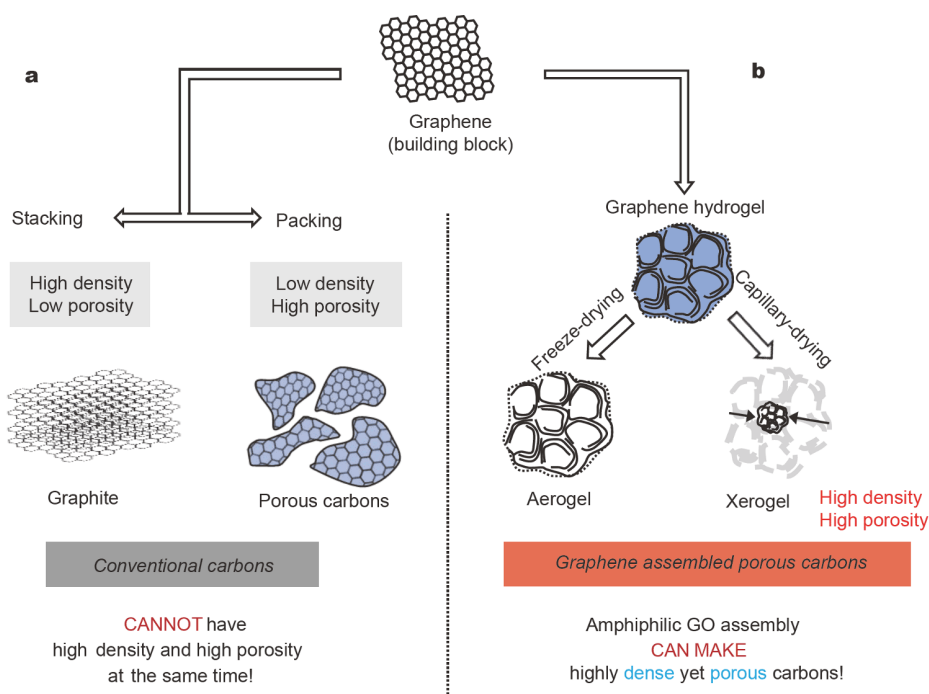[*] Corresponding author (email: qhyangcn@tju.edu.cn)

Figure 1 (a) Two typical assembly models for conventional carbon materials, which can be regarded as assemblies with graphene as building blocks; (b) preparation of different porous carbons by removing residual solvents in different ways.

philic oxygen-containing group-decorated edges [19,20]. Therefore, these amphiphilic GO sheets can be readily dispersed in water and act as a surfactant, allowing their controlled assembly into various graphene-based structures [21–25]. Reduced GO (r-GO) hydrogels can be easily obtained by the reduction-induced processes of GO suspension, like chemical reduction [26] or hydrothermal treatment [27,28], and have a 3D cross-linked framework with high surface utilization and processibility. There are two typical drying methods for r-GO hydrogels, supercritical drying and freeze-drying, as shown in Fig. 1b. These methods are used to obtain r-GO aerogels, which retain the pore structure, the morphology and volume of the original hydrogel due to the weak interaction between the ice/supercritical fluid and the r-GO sheets [29–31]. However, the density of the formed aerogels is quite low and is inappropriate for practical energy storage.

Another approach is evaporation drying to produce xerogels [32], where water evaporation causes the dramatic shrinkage of the network or even cracks the xerogels into powders. However, the monolithic r-GO xerogels obtained after shrinkage retain both high porosity and density of the precursor due to the flexibility of the r-GO sheets and the stability of the carbon network [12,15,33]. The strong interaction between the water and the r-GO layers causes the shrinkage of the preformed network. During the water evaporation, the r-GO network shrinks into compact but still porous xerogels. Interestingly, the r-GO xerogel has almost the same surface area as the r-GO aerogel [34]. With different drying approaches, the r-GO hydrogels produce distinct microstructures with different densities, because of the different interactions between the r-GO sheets and the removed media [35,36]. Water has much stronger interaction with the flexible r-GO sheets compared with ice, which has almost no interaction with the network. Therefore the mechanism that the shrinkage of the graphene network is caused by capillary forces is proposed [12], which has also been used to explain the compression of graphene gel films [12,33]. The shrinkage of r-GO hydrogels is not yet clearly illustrated and there is still no full understanding of how the capillary forces work. Here, the proposed "capillary" shrinkage of r-GO hydrogels was investigated using two solvents, water and 1,4-dioxane.

EXPERIMENTAL SECTION

Preparation of the solvated GO frameworks with different water-miscible organic solvents
GO was prepared from graphite powder by a modified Hummers method. A GO colloidal suspension (2 mg mL^{-1}) was prepared by the ultrasonication of GO

powder in ultra-pure water for 2 h, followed by centrifugation (3800 rpm for 10 min) to remove the thick layers. The GO colloidal suspension was placed in a Teflon-lined autoclave, and treated by a hydrothermal process at 180°C for 6 h to produce a free-standing, black cylindrical r-GO hydrogel.

The r-GO hydrogel was immersed in fresh water-miscible organic solvent at 40°C for 4 h to displace the trapped water. This process was performed three times to guarantee a complete solvent exchange. Then it was dried at 70°C under atmospheric pressure and the r-GO monolith was obtained. The samples are denoted as EtOH-G, Acetone-G, Diox-G, DMF-G, EG-G for exchange solvents ethanol, acetone, 1,4-dioxane, N,N-dimethylformamide (DMF), and ethylene glycol, respectively. The dried r-GO hydrogel is denoted as HPGM.

Material characterizations

Fourier transform infrared spectrum (FTIR) was measured using a Bruker 6700 spectrometer. Scanning electron microscopy (SEM) observations were performed on a Hitachi S-4800 (Hitachi, Japan). Nitrogen adsorption was measured using a BEL mini-instrument, and the desolvated r-GO hydrogels were outgassed at 473 K for 12 h before the N_2 adsorption measurements. The specific surface areas, pore volumes and pore size distributions (PSD) were obtained from the adsorption isotherm by the Brunauer-Emmett-Teller (BET) method and density

functional theory (DFT) (N_2 at 77 K on carbon, slit/cylindr./spherical pores, QSDFT). X-ray diffraction (XRD) was conducted at room temperature using a Bruker D-8 instrument with Cu Kα radiation (λ= 0.154056 nm). The surface tension (γ^{lg}) of the liquid was measured at 25°C with a Kruss K11 instrument. The bulk densities of desolvated r-GO hydrogels were determined by Archimedes principle with a balance (METTLER TOLEDO XS205) equipped with accessories for the density determination.

RESULTS AND DISCUSSION

Typically, an integral r-GO hydrogel (Fig. 2a) can be prepared by hydrothermal treatment of a GO suspension [12]. The r-GO sheets retain a number of oxygen-containing functional groups as shown in Figs S1, S2, which generate interactions with solvents or other molecules [37]. An interconnected 3D porous r-GO network was formed according to the SEM observation of r-GO hydrogels after freeze-drying (Fig. S3).

Through the evaporation of water, a capillary force between the r-GO sheets and the solvent compacts the 3D porous network and makes the hydrogel shrink into a dense r-GO monolith (HPGM, Fig. 2b). 1,4-Dioxane (Fig. S4) is a heterocyclic organic compound with good water solubility and has very similar properties with water, such as density, boiling point and viscosity, which guarantees the similar evaporation environment. The only major difference between water and 1,4-dioxane is the surface tension which is 32.85 mN m^{-1} at 25°C for
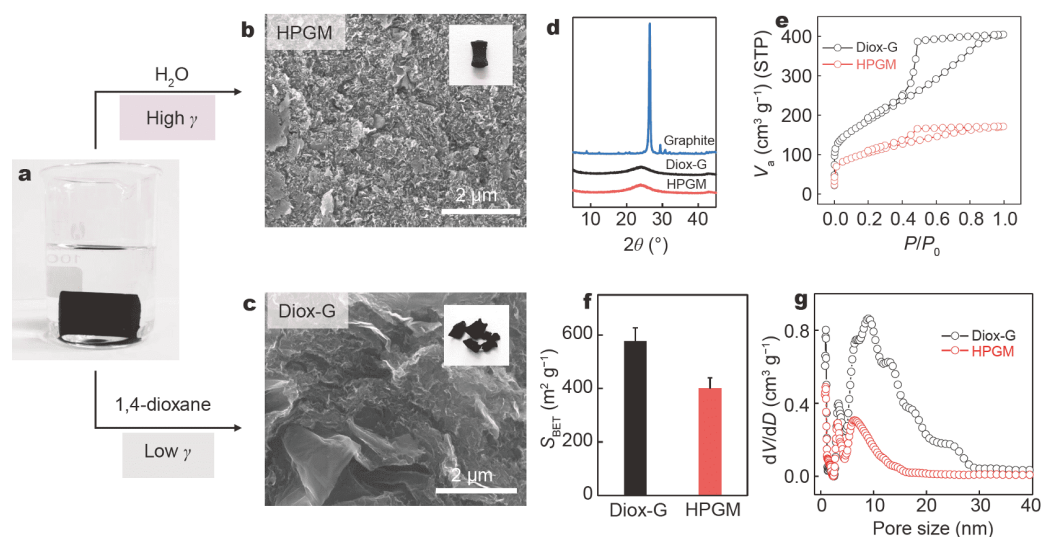

Figure 2 Capillary shrinkage of r-GO hydrogels using two solvents with almost the same boiling point yet different surface tensions. (a) An integral r-GO hydrogel obtained after hydrothermal treatment; (b, c) SEM images and inset photos of the monoliths obtained by immersion of patent hydrogels in water or 1,4-dioxane for solvent-exchange and then dried; (d) XRD patterns of these r-GO monoliths; (e) N_2 adsorption-desorption isotherms; (f) BET surface area and (g) PSD of the resulting HPGM and Diox-G.

1,4-dioxane (γ_{Diox}) [38], much lower than that of water (γ_{Water}, 71.96 mN m^{-1}, 25°C) (Scheme S1) [39]. The r-GO hydrogel was soaked in water or 1,4-dioxane four times to fully exchange the solvent. After drying, the trapped solvents (water or 1,4-dioxane) were evaporated and the desolvated r-GO shrunk into bulk material, denoted as HPGM and Diox-G, respectively. During the water evaporation, r-GO sheets were gradually compacted and shrunk into an integral dense monolith (inset photo in Fig. 2b). In contrast, those in 1,4-dioxane were less squeezed and the product split into several pieces (inset photo in Fig. 2c), due to the lower surface tension of the solvent and its smaller capillary interaction with the r-GO sheets. The SEM images also show that the r-GO sheets in Diox-G are irregularly stacked (Fig. 2c) compared with the more uniformly compacted r-GO sheets in HPGM (Fig. 2b). More importantly, no apparent graphite (002) peak was found in the XRD patterns (Fig. 2d) of Diox-G and HPGM, indicating that the r-GO sheets were in a disordered arrangement and not restacked into graphitic structures [33]. The nitrogen adsorption/desorption measurements indicate that some micropores and small mesopores remain after the capillary shrinkage. Both the HPGM and Diox-G samples show classical I/IV type isotherms with a type H2 hysteresis loop (Fig. 2e) [40], demonstrating the existence of abundant micropores and mesopores. The higher adsorption capacity at low relative pressure in Diox-G indicates its larger surface area, which was further calculated by the BET method and shown in Fig. 2f. The average specific surface area (S_{BET}) of Diox-G (576 m^2 g^{-1}) is higher than that of the HPGM (400 m^2 g^{-1}). Except for the micropores, the center of PSD curve increases from ~6.4 nm (HPGM) to 8.9 nm (Diox-G), as determined by the DFT method (Fig. 2g). These results indicate that the capillary shrinkage in different solvents generates distinct changes in the resulting r-GO microstructures. The major difference between water and 1,4-dioxane is the surface tension and the solvent with higher surface tension shows the stronger capillary interactions with r-GO sheets, resulting in a larger shrinkage with a smaller pore size and a lower specific surface area.

The schematic in Fig. 3a illustrates the solvent evaporation and capillary shrinking process in r-GO hydrogels. The r-GO sheets are cross-linked, forming a 3D framework with continuous capillary channels. The r-GO sheets are flexible and robust and can withstand crumpling or squeezing during water evaporation and the oxygen-containing functional groups on them have strong hydrogen bonding with the water molecules [41].

The hydrogel contains tiny grooves so that water in them exerts capillary forces on the r-GO sheets during water evaporation as shown in Fig. 3b. Different solvents exert different capillary pressure (P_c), causing different volume changes (δ_v). The relationship between the volume change and the capillary pressure applied to the r-GO hydrogel can be expressed as follows [42]:

$$P_c = -\frac{2\gamma\cos\theta}{r}, \qquad (1)$$

$$\delta_v \sim \frac{P_c}{K} = \frac{-2\gamma\cos\theta}{rK}, \qquad (2)$$

where the capillary pressure is defined as a function of the solvent surface tension (γ), contact angle (θ), and pore radius (r) according to the Young-Laplace equation. The bulk modulus (K) is constant and mainly depends on the structural properties of the r-GO hydrogel framework. Therefore, higher surface tension and smaller pore size generate a larger capillary pressure.

As shown in Fig. 3b, the generated capillary pressure is directed to the concave liquid surface, and can be resolved into two directions. F_X is the force perpendicular to the r-GO sheet and F_Y is the force along the r-GO sheet. In capillary evaporation, F_Y is the driving force for the removal of water from the framework and F_X mainly compacts the r-GO sheets, inducing shrinkage of the hydrogel. A larger surface tension generates a larger F_X for a stronger compacting force. Eventually, the porous network of flexible r-GO sheets shrinks into a dense yet porous r-GO monolith with water evaporation. The 1,4-dioxane also causes capillary shrinkage of r-GO hydrogel, but, due to the lower surface tension, the shrinkage is less and more mesopores are preserved, giving a higher pore volume.

The above discussion indicates that the surface tension and its associated capillary forces play a determining role in the evaporation-induced shrinkage of the r-GO hy-
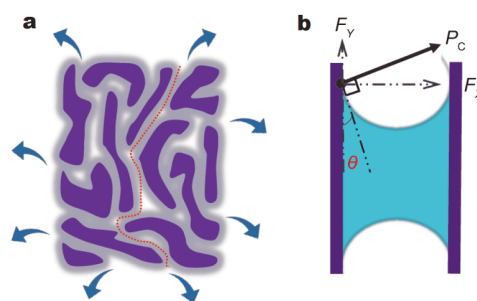

Figure 3 Capillary shrinkage of the r-GO hydrogel during solvent evaporation. (a) Schematic of the r-GO hydrogel capillary shrinkage process; (b) capillary force exerted on the r-GO sheets during solvent evaporation.

drogel. To verify this assumption, a series of water-miscible organic solvents with different surface tensions were investigated to controllably adjust the microstructures of the desolvated r-GO hydrogel. The exchange solvents were ethanol, acetone, DMF and ethylene glycol, and the resulting samples are denoted as EtOH-G, Acetone-G, DMF-G and EG-G, respectively. These solvents need to be fully exchanged otherwise residual water will affect the results (Figs S5, S6). The macroscopic morphologies of the resulting samples are obviously different as shown in Fig. 4a, where the solvents with higher surface tension induce more compact bulk materials with fewer cracks or broken pieces. For a lower-surface-tension-solvent evaporation, the capillary force is relatively weak, leading to insufficient densification of r-GO assembly and a mechanically unstable structure. SEM observations show

that the debris also has an interconnected and dense framework without large voids (Fig. S7). All these samples have no sharp graphite peaks in the XRD patterns (Fig. S8), indicating the r-GO sheets are not restacked even after strong capillary compression.

The pore structures of these desolvated r-GO hydrogels were compared (Fig. 4b) and they showed quite different adsorption isotherms. The r-GO monoliths produced by the solvents with lower surface tension show a higher adsorption capacity and a negative correlation between the specific surface area and the liquid surface tension (Fig. 4c). The specific surface area increases from 400 m^2 g^{-1} (HPGM) to 635 m^2 g^{-1} (EtOH-G) when the surface tension decreases from 71.96 mN m^{-1} (water) to 21.27 mN m^{-1} (EtOH). While the monoliths show a larger average pore size and a larger pore volume in solvents
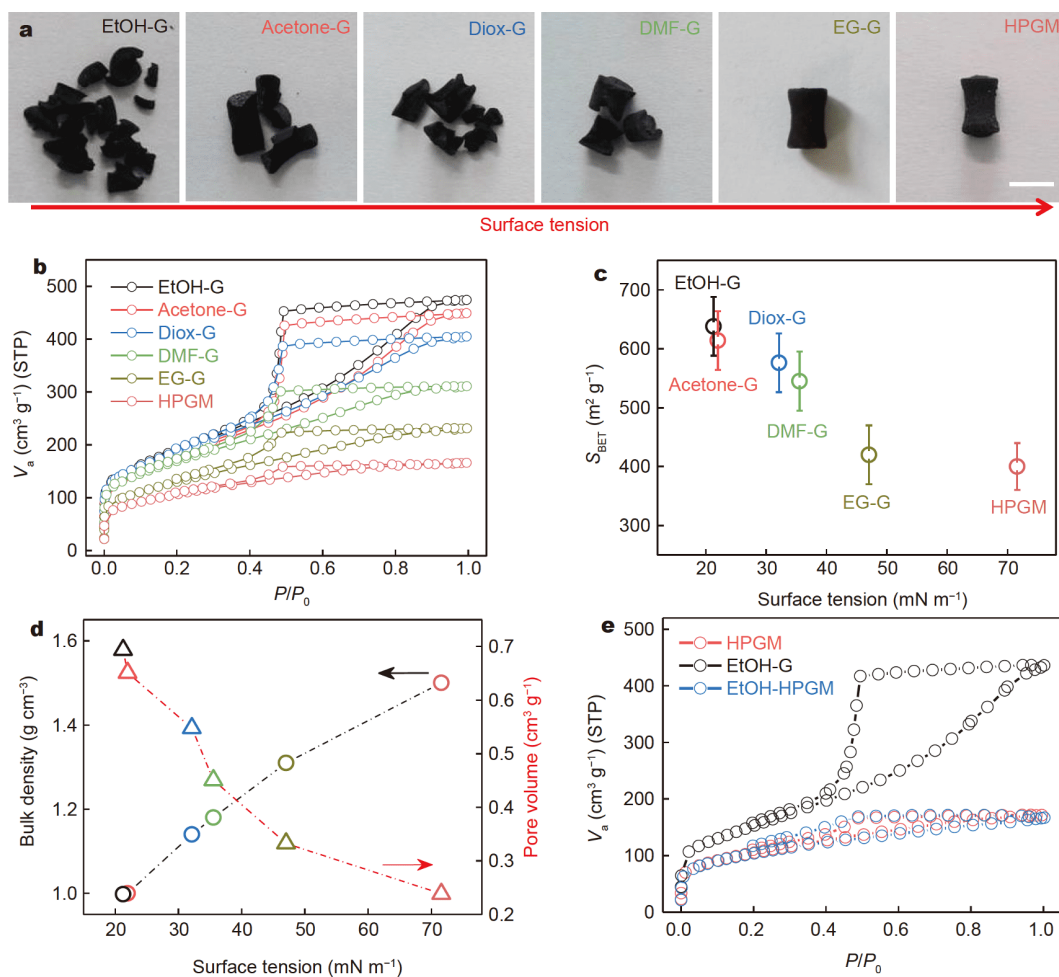

Figure 4 Characterizations of the r-GO monoliths obtained in solvents with different surface tensions. (a) Photos of the r-GO monoliths after solvent evaporation; (b) N$_2$ adsorption/desorption isotherms of the desolvated r-GO monoliths; (c) relationship between the BET surface area and solvent surface tension; (d) bulk density and cumulative pore volume of the desolvated r-GO monoliths as a function of solvent surface tension; (e) the EtOH-G monolith can be further densified to EtOH-HPGM by second drying after immersion in water. It has similar isotherms to HPGM.

with higher surface tension, with no significant difference in the amount and size of micropores (below 2 nm) (Figs S9, S10). This is also confirmed by the transmission electron microscopey (TEM) images in Fig. S11. Moreover, the density of the resulting monolith decreases with lower solvent surface tension as shown in Fig. 4d where HPGM has the highest density and EtOH-G has the lowest. Among all volatile liquids which have good wettability with the rGO sheets, the surface tension of water is the largest; therefore the density of the bulk material obtained using water as the solvent is the highest under the solvent capillary evaporation. These results show that the densification of r-GO frameworks and their microstructures are closely related to the surface tension of the trapped solvent. Generally, the ratio of different surface-tension solvents determines the capillary force and the solvent exchange degree would also affect the capillary shrinkage of the hydrogel. But the surface tension can be stabilized with a sufficient solvent exchange. By controlling the solvent, the shrinkage of the hydrogel can be manipulated to precisely control the density and porosity of the resulting r-GO monolith.

Interestingly, the less compact r-GO monoliths can be further densified by a second capillary shrinkage using another solvent with higher surface tension. As shown in Fig. 4e, EtOH-G with abundant mesopores was immersed in water which was then evaporated (denoted as EtOH-HPGM). The large mesopores in EtOH-G became smaller in EtOH-HPGM, which gave almost the same isotherms as HPGM, showing that the water permeated the capillary channels and further densified the resulting microstructure through capillary pressure. The desolvated r-GO hydrogels obtained in other solvents (like acetone or DMF) could also be densified through a secondary solvent-exchange process in water as shown in Fig. S12. Such an approach provides an effective way to densify r-GO structures and has great potential for improving the volumetric performance of porous materials.

CONCLUSIONS
In summary, the shrinkage of a r-GO hydrogel induced by evaporation is driven by the surface tension of the trapped solvent and the associated capillary force that is regulated by the interfacial interaction between the r-GO sheets and the solvent, and therefore this evaporation-induced drying is defined here as capillary drying. Solvents with a higher surface tension generate a stronger capillary force during evaporation, which compacts the r-GO framework into a dense yet porous material. By using solvents with different surface tensions, the micro-

structure of the resulting materials can be precisely manipulated and densified, realizing an excellent balance of the density and porosity in materials not limited to carbon materials [43], and giving the particular potential for high volumetric performance in practical devices.

1 Geim AK, Novoselov KS. The rise of graphene. Nat Mater, 2007, 6: 183–191
2 Allen MJ, Tung VC, Kaner RB. Honeycomb carbon: a review of graphene. Chem Rev, 2009, 110: 132–145
3 Ye C, Zhou X, Pu D, et al. Rapid cycling of reactive nitrogen in the marine boundary layer. Nature, 2016, 532: 489–491
4 Ju Z, Li P, Ma G, et al. Few layer nitrogen-doped graphene with highly reversible potassium storage. Energy Storage Mater, 2018, 11: 38–46
5 Liu L, Lin Z, Chane-Ching JY, et al. 3D rGO aerogel with superior electrochemical performance for K–Ion battery. Energy Storage Mater, 2019, 19: 306–313
6 Raymundo-Piñero E, Leroux F, Béguin F. A high-performance carbon for supercapacitors obtained by carbonization of a seaweed biopolymer. Adv Mater, 2006, 18: 1877–1882
7 Zhang C, Lv W, Tao Y, et al. Towards superior volumetric performance: design and preparation of novel carbon materials for energy storage. Energy Environ Sci, 2015, 8: 1390–1403
8 Wang Q, Yan J, Fan Z. Carbon materials for high volumetric performance supercapacitors: design, progress, challenges and opportunities. Energy Environ Sci, 2016, 9: 729–762
9 Liu C, Yan X, Hu F, et al. Toward superior capacitive energy storage: recent advances in pore engineering for dense electrodes. Adv Mater, 2018, 30: 1705713
10 Zhou Y, Ghaffari M, Lin M, et al. High volumetric electrochemical performance of ultra-high density aligned carbon nanotube supercapacitors with controlled nanomorphology. Electrochim Acta, 2013, 111: 608–613
11 Murali S, Quarles N, Zhang LL, et al. Volumetric capacitance of compressed activated microwave-expanded graphite oxide (a-MEGO) electrodes. Nano Energy, 2013, 2: 764–768
12 Tao Y, Xie X, Lv W, et al. Towards ultrahigh volumetric capacitance: graphene derived highly dense but porous carbons for supercapacitors. Sci Rep, 2013, 3: 2975–2982
13 Li H, Tao Y, Zheng X, et al. Compressed porous graphene particles for use as supercapacitor electrodes with excellent volumetric performance. Nanoscale, 2015, 7: 18459–18463
14 Zhang C, Liu DH, Lv W, et al. A high-density graphene–sulfur assembly: a promising cathode for compact Li–S batteries. Nanoscale, 2015, 7: 5592–5597
15 Xu Y, Tao Y, Zheng X, et al. A metal-free supercapacitor electrode material with a record high volumetric capacitance over 800 F cm^{-3}. Adv Mater, 2015, 27: 8082–8087
16 Zhang C, Yang QH. Packing sulfur into carbon framework for high volumetric performance lithium-sulfur batteries. Sci China Mater, 2015, 58: 349–354
17 Qin L, Zhai D, Lv W, et al. Dense graphene monolith oxygen cathodes for ultrahigh volumetric energy densities. Energy Storage Mater, 2017, 9: 134–139
18 Zhang J, Lv W, Tao Y, et al. Ultrafast high-volumetric sodium

storage of folded-graphene electrodes through surface-induced redox reactions. Energy Storage Mater, 2015, 1: 112–118

19 Dreyer DR, Park S, Bielawski CW, et al. The chemistry of graphene oxide. Chem Soc Rev, 2010, 39: 228–240

20 Kim J, Cote LJ, Kim F, et al. Graphene oxide sheets at interfaces. J Am Chem Soc, 2010, 132: 8180–8186

21 Dikin DA, Stankovich S, Zimney EJ, et al. Preparation and characterization of graphene oxide paper. Nature, 2007, 448: 457–460

22 Zhao Y, Hu C, Hu Y, et al. A versatile, ultralight, nitrogen-doped graphene framework. Angew Chem Int Ed, 2012, 51: 11371–11375

23 Ge J, Shi LA, Wang YC, et al. Joule-heated graphene-wrapped sponge enables fast clean-up of viscous crude-oil spill. Nat Nanotech, 2017, 12: 434–440

24 Shao JJ, Lv W, Yang QH. Self-assembly of graphene oxide at interfaces.. Adv Mater, 2014, 26: 5586–5612

25 Cong HP, Chen JF, Yu SH. Graphene-based macroscopic assemblies and architectures: an emerging material system. Chem Soc Rev, 2014, 43: 7295–7325

26 Chen W, Yan L. In situ self-assembly of mild chemical reduction graphene for three-dimensional architectures. Nanoscale, 2011, 3: 3132

27 Xu Y, Sheng K, Li C, et al. Self-assembled graphene hydrogel via a one-step hydrothermal process. ACS Nano, 2010, 4: 4324–4330

28 Xu Y, Lin Z, Zhong X, et al. Solvated graphene frameworks as high-performance anodes for lithium-ion batteries. Angew Chem Int Ed, 2015, 54: 5345–5350

29 Padmajan Sasikala S, Poulin P, Aymonier C. Prospects of supercritical fluids in realizing graphene-based functional materials. Adv Mater, 2016, 28: 2663–2691

30 Qiu L, Liu JZ, Chang SLY, et al. Biomimetic superelastic graphene-based cellular monoliths. Nat Commun, 2012, 3: 1241–1246

31 Sun H, Xu Z, Gao C. Multifunctional, ultra-flyweight, synergistically assembled carbon aerogels. Adv Mater, 2013, 25: 2554–2560

32 Job N, Théry A, Pirard R, et al. Carbon aerogels, cryogels and xerogels: Influence of the drying method on the textural properties of porous carbon materials. Carbon, 2005, 43: 2481–2494

33 Yang X, Cheng C, Wang Y, et al. Liquid-mediated dense integration of graphene materials for compact capacitive energy storage. Science, 2013, 341: 534–537

34 Tao Y, Kong D, Zhang C, et al. Monolithic carbons with spheroidal and hierarchical pores produced by the linkage of functionalized graphene sheets. Carbon, 2014, 69: 169–177

35 Jia X, Zhang C, Liu J, et al. Evolution of the effect of sulfur confinement in graphene-based porous carbons for use in Li–S batteries. Nanoscale, 2016, 8: 4447–4451

36 Sierra U, Álvarez P, Santamaría R, et al. A multi-step exfoliation approach to maintain the lateral size of graphene oxide sheets. Carbon, 2014, 80: 830–832

37 Nair RR, Wu HA, Jayaram PN, et al. Unimpeded permeation of water through helium-leak-tight graphene-based membranes. Science, 2012, 335: 442–444

38 Hovorka F, Schaefer RA, Dreisbach D. The system dioxane and water. J Am Chem Soc, 1936, 58: 2264–2267

39 Baker NB, Gilbert EC. Surface tension in the system hydrazine—water at 25°. J Am Chem Soc, 1940, 62: 2479–2480

40 Thommes M, Kaneko K, Neimark AV, et al. Physisorption of gases, with special reference to the evaluation of surface area and pore size distribution (IUPAC Technical Report). Pure Appl Chem, 2015, 87: 1051–1069

41 Steiner T. The hydrogen bond in the solid state. Angew Chem Int Ed, 2002, 41: 48–76

42 Xu X, Zhang Q, Yu Y, et al. Naturally dried graphene aerogels with superelasticity and tunable Poisson's ratio. Adv Mater, 2016, 28: 9223–9230

43 Shang T, Lin Z, Qi C, et al. 3D macroscopic architectures from self-assembled MXene hydrogels. Adv Funct Mater, 2019, 29: 1903960

Author contributions   Yang QH conceived and supervised the study. Qi C and Tao Y designed the experiment and Qi C carried out it. Qi C, Luo C, Tao Y and Yang QH discussed the data. Lv W, Zhang C, Deng Y, Li H, Han J, Ling G provided the technical support and commented the results.

Conflict of interest   The authors declare no conflict of interest.

Supplementary information   Experimental details and supporting data are available in the online version of the paper.

Changsheng Qi received his Bachelor's degree and Master's degree of applied chemistry from the North University of China in 2005 and 2008, respectively. He is a PhD candidate under the guidance of Prof. Quan-Hong Yang. His research interest focuses on the liquid phase assembly and mechanism of GO, and its applications.

Chong Luo received his Bachelor's degree of materials science and engineering from the Central South University in 2013 and now is a PhD candidate under the guidance of Prof. Quan-Hong Yang and Prof. Wei Lv. His research interest focuses on the liquid phase assembly of GO and mechanism study on energy storage.

Ying Tao is an associate professor at the School of Chemical Engineering and Technology at Tianjin University. Her main research interests focus on the assembly of low dimensional materials, carbon-based materials and their applications in electrochemical energy storage and environmental remediation.

Quan-Hong Yang joined Tianjin University as a full professor in 2006 and became a Chair Professor in the same university in 2016. His research focuses on novel functional carbon materials with the applications in energy and environmental fields. Specifically, he has made significant advances in high volumetric performance EES devices and the catalysis in lithium-sulfur batteries. See http://nanoyang.tju.edu.cn for more details about Nanoyang Group.

氧化石墨烯水凝胶的毛细收缩机制

戚昌盛[1,4†], 罗冲[2†], 陶莹[1,4†], 吕伟[2], 张辰[3], 邓亚茜[2], 李欢[1,4], 韩俊伟[1,4], 凌国维[3], 杨全红[1,4*]

摘要 以两亲性氧化石墨烯为结构单元, 可控组装构建三维网络石墨烯水凝胶, 通过溶剂蒸发驱动网络致密化, 获得高密多孔碳, 解决了传统多孔碳电极体积容量低的应用瓶颈. 本文旨在探究氧化石墨烯水凝胶致密化机理, 阐明了毛细作用力是使溶剂脱出并引发石墨烯网络收缩的驱动力. 溶剂表面张力决定毛细作用力, 因此通过调节溶剂表面张力或采用不同表面张力的溶剂, 可以实现"孔"与"密"的"收放自如"调控, 从而得到不同密度和孔隙率的高密多孔碳, 实现高密和多孔连续精确调控. 氧化石墨烯水凝胶的毛细收缩也为纳米材料致密化提供了方法论支持.